*Rev. Roum. Sci. Techn.– Électrotechn. et Énerg.*
Vol. **67**, *3*, pp. 331–335, Bucarest, 2022

# IMPLEMENTATION FOR SEVENTH-ORDER LOW-PASS CAUER FILTER EMPLOYING SECOND-GENERATION CURRENT-CONTROLLED CONVEYOR

YONG-AN LI[1,2], JING-QIANG HOU[2]

**Keywords: Seventh-order low-pass filter; Cauer filter; Current-mode circuits; Second-generation current-controlled conveyor.**

**After utilizing adjoint network theory, Bruton transform, frequency-dependent negative resistance (FDNR), component replacement method, and frequency and impedance scaling, a seventh-order low-pass Cauer filter from the normalized RLC prototype circuit is converted to the current-mode filter with $f_c$ = 15 kHz, $f_s$ = 18.78 kHz, $A_{max}$ = 0.28 dB, and $A_{min}$ = 60 dB, which includes only six second-generation current-controlled conveyors (CCCIIs) and grounded capacitors, does not need any matched conditions, and adjusting bias currents of the CCCIIs can control performances of the filter, The computer simulation has verified the correctness of this design.**

## 1. INTRODUCTION

The Cauer filter, for its inventor Wilhelm Cauer, is also known as the Elliptic filter because it is obtained according to the elliptic function approximation criterion. The Cauer filter goes further than the Chebyshev approach by setting ripples in both the passband and the stopband for a clearer transition-band characteristic. Therefore, the Cauer filter has been widely used in digital and analog signal processing and telecommunication systems such as channel equalization, noise reduction, radar, audio processing, speech signal processing, video processing, biomedical signal processing, *etc*. [1–9]. Even though the Cauer filter using traditional operational amplifiers (Op Amps) has been investigated by Franco [10], this filter is typically a voltage-mode circuit rather than a current-mode circuit. While a higher-order multifunction filter using a current differencing buffered amplifier (CDBA) is a current-mode circuit, its parameters cannot be adjusted electronically [11].

The Cauer filter using current differencing transconductance amplifiers (CDTAs), modified CDTAs (MCDTAs), and operational transconductance amplifiers (OTAs) should be current-mode circuits, and its behavioral parameters can be tuned electrically [12–15]. Unfortunately, these reported circuits employ a cascade design, making the overall response particularly sensitive to parameter variations of individual stages resulting from thermal drift, tolerance, and aging. High-*Q* stages are especially noteworthy because even a small variation in component parameters may seriously affect the response of the whole cascade.

These weaknesses need to be overcome to obtain a high-performance Cauer filter. Filters from doubly terminated series resonant RLC ladder, as we know it, is a tightly coupled circuit, where sensitivity is distributed across all elements, rather than being limited to a few specific elements. Therefore, this circuit is the basis for obtaining high-performance filters.

On the other hand, the second-generation current-controlled conveyor (CCCII) was first proposed by Fabre in 1996 in bipolar technology [16]. Since then, all kinds of current-mode circuits employing the CCCII, such as the gyrator circuit, analog filter, and analog oscillator, have emerged [17–25]. This shows that the CCCII is a fundamental, general, and versatile current-mode device [26–29]. Unfortunately, so far, seventh-order filters employing the CCCII as an active element, especially the low-pass Cauer filter, are rarely reported. Therefore, this is a problem to be researched further.

This work starts with a classic seventh order Cauer passive filter, the normalized RLC prototype circuit, with maximum passband ripple $A_{\max}$= 0.28 dB, passband cutoff frequency $f_c$ =15 kHz, minimum stopband attenuation $A_{\min}$ = 60 dB, and stopband cutoff frequency $f_s$ = 18.78 kHz.

First, the classic voltage-mode passive filter is converted to the current mode filter through the adjoint network theory, then the passive inductance in the filter is removed through the Bruton transform, then the *D* element in the filter is replaced with the frequency-dependent negative resistance (FDNR) based on CCCII, and finally, the seventh-order current-mode active filter is implemented using the frequency and impedance scaling. The simulation of the designed circuit shows that the filter is correct and effective. The filter designed in the paper is compared with several filters reported in the references, and the results are summarized in Table 1.

## 2. DESIGN BASIS

### 2.1. CONCISE DESCRIPTION OF CCCII

Figure 1a – b shows symbols of the CCCII+ and CCCII-, respectively. Ideally, the CCCII can be described by the following equations:

$$I_y = 0,\ \ V_x = R_x I_x + V_y,\ \ I_z = \pm I_x, \tag{1}$$

where the plus sign in the third formula means the CCCII+, and the minus sign indicates the CCCII-. For the CCCII using bipolar technology, $R_X$, representing the parasitic resistances at the *x* input terminal, can be written as

$$R_X = \frac{V_T}{2I_B}, \tag{2}$$

where $I_B$ is the bias current of the CCCII and $V_T$ is the usual thermal voltage.

---

[1] School of Physics and Electronic Engineering, Xianyang Normal University, Xianyang 712000, Shaanxi, China
Corresponding author: lya6189@tom.com
[2] School of Information Engineering, Shaanxi Institute of International Trade & Commerce, Xi'an 712046, Shaanxi, China
E-mail: 670633210@qq.com

*Table 1*

Comparison with existing higher order filters

| Ref | Active device | No. of active devices | No. of external resistors | Grounded C only | Electronic control | Current mode | Order of Cauer filter |
|---|---|---|---|---|---|---|---|
| [10] | Op Amp | 7 | 18 | No | No | No | 7 |
| [11] | CDBA | 1 | 9 | No | No | No | 5 |
| [12] | MCDTA | 6 | 4 | Yes | Yes | Yes | 6 |
| [13] | MCDTA | 6 | 2 | Yes | Yes | Yes | 6 |
| [14] | OTA | 12 | 0 | Yes | Yes | No | 4 |
| [15] | OTA | 7 | 0 | Yes | Yes | No | 3 |
| [26,27] | CCCII | 6 | 0 | Yes | Yes | Yes | 4 |
| Proposed filter | CCCII | 6 | 6 | Yes | Yes | Yes | 7 |

The current buffer shown in Fig. 1(c) employs one CCCII. Ideally, the output resistance of the circuit is infinite, and the input resistance is $R_X$. However, if $I_B$ is set to 1 mA, then $R_X = 13\ \Omega$, which is already very small, so this circuit is close in performance to an ideal current buffer.

Fig. 1(d) represents a CCCII-employed FDNR with a lossy resistance [30–31]. Ideally, its input impedance is

$$Z_D = R_{X1} - \frac{1}{\omega^2 D} = \frac{V_T}{2I_{B1}} - \frac{1}{\omega^2 D},$$

$$R_{X1} = \frac{V_T}{2I_{B1}},\ D = C_1 C_2 R_{X2} = \frac{C_1 C_2 V_T}{2I_{B2}}. \qquad (3)$$

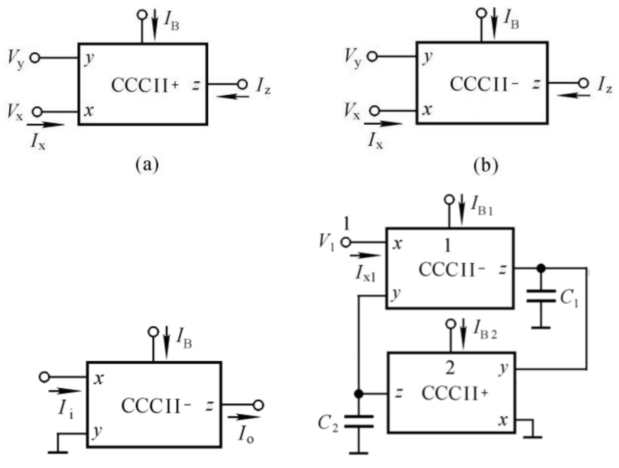

(a) (b)

(c) (d)

Fig. 1 – Concise description of the CCCII: a) symbol for CCCII+; b) symbol for CCCII-; c) current buffer employing CCCII; d) FDNR employing CCCII- with a lossy resistance.

It can be observed that the circuit is equivalent to a resistor and a $D$ component. This resistance can be tuned by changing $I_{B1}$ and changing $I_{B2}$ can also tune the value of $D$ component. This is the basis for designing current-mode circuits with electronic regulation.

## 2.2 CLASSIC RLC PROTOTYPE FILTER

If the analog signals that will be blocked are very near in frequency to those that are hoped to pass, a general filter is not suitable for this task because of its unsharp cutoff characteristics, however, a higher-order filter circuit may then be needed. A classic seventh-order passive filter shown in Fig. 2 is implemented using suitable filter tables or computer programs [10]. It belongs to the doubly terminated series resonant *RLC* prototype network. Because the inductances serve as shorts and the capacitances as opens at low frequencies, the signal, from the input to the output of the ladder, passes directly through and the gain for low frequencies is 0.5. Because the capacitances serve as shorts at high frequencies, the behavior of the ladder is mainly inductive; it then attenuates high-frequency signals. Because the series resonance of the *LC* elements in each shunt can appear at intermediate frequencies, giving a series of notches, one for each shunt. Therefore, the ladder is a low-pass filter that includes notches or an elliptic low-pass filter. To be sure, filters from the doubly terminated ladder retain the lowest passive sensitivities. Considering the sensitivity and the rich professional information available in the field of passive filter design, we have this thought for designing the seventh-order low-pass Cauer filter employing the CCCII as an active element.

## 3. **DESIGN PROCEDURE**

The circuit in Fig. 2 is the starting point for the design. Utilizing the adjoint network theory in the circuit of Fig. 2, the open-circuit voltage at the output is changed into an input current source; the input voltage source is transformed into the short-circuit current at the output, then the voltage-mode circuit of Fig. 2 is converted to the current-mode circuit of Fig. 3.

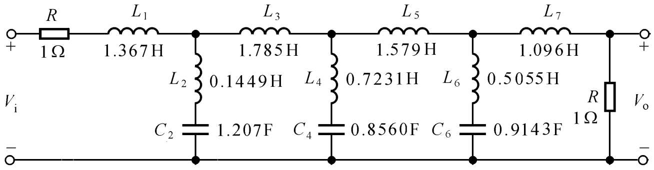

Fig. 2 – Classic seventh order RLC filter prototype.

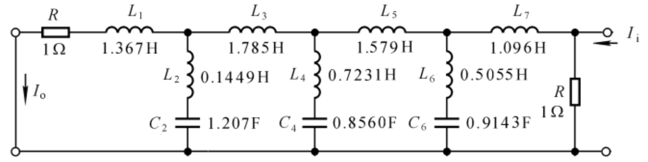

Fig. 3 – The adjoint circuit of the filter of Fig. 2.

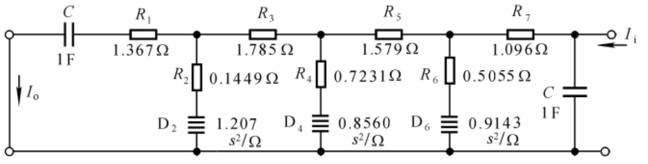

Fig. 4 – CRD equivalent filter of Fig. 3.

According to the Bruton transformation, if the resistance value of $R$ is replaced by a capacitance of value $1/R$; the inductance value of $L$ is replaced by the resistance of value $L$; the capacitance value of $C$ is replaced by the $D$ element of value $C$, then the transfer function of the network remains unchanged, as shown in Fig. 4.

For obtaining the active filter employing the CCCII, the resistance and $D$ elements of each leg in Fig. 4 can be substituted by the circuit in Fig. 1(d), and the filter of Fig. 5 thus be received.

It should be noted that element values of the filter of Fig. 5 are normalized, and then the normalized component values satisfy:

$$R_N=\frac{R}{k_z},\quad C_N=k_z\omega_c C,\quad D_N=k_z\omega_c^2 D. \tag{4}$$

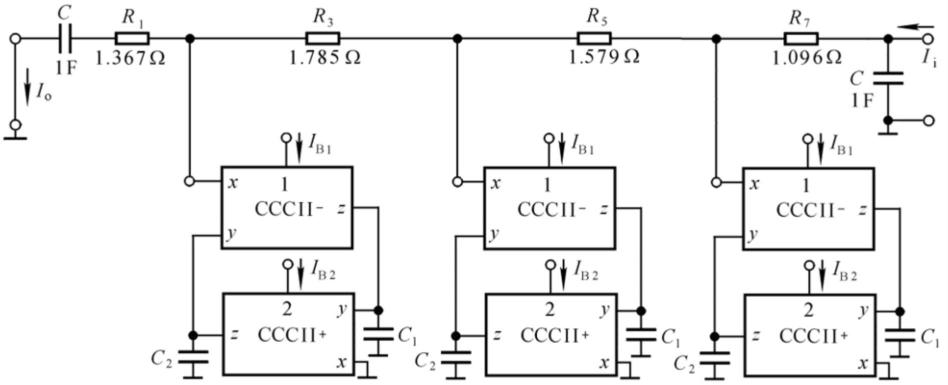

Fig. 5 – Active realization using FDNRs. Leftmost: $I_{NB1}$ = 89.72×$10^{-3}$ A, $I_{NB2}$ = 10.77×$10^{-3}$ A; center: $I_{NB1}$ = 17.97×$10^{-3}$ A, $I_{NB2}$ = 15.19×$10^{-3}$ A; rightmost: $I_{NB1}$ = 25.72×$10^{-3}$ A, $I_{NB2}$ = 14.22×$10^{-3}$ A.

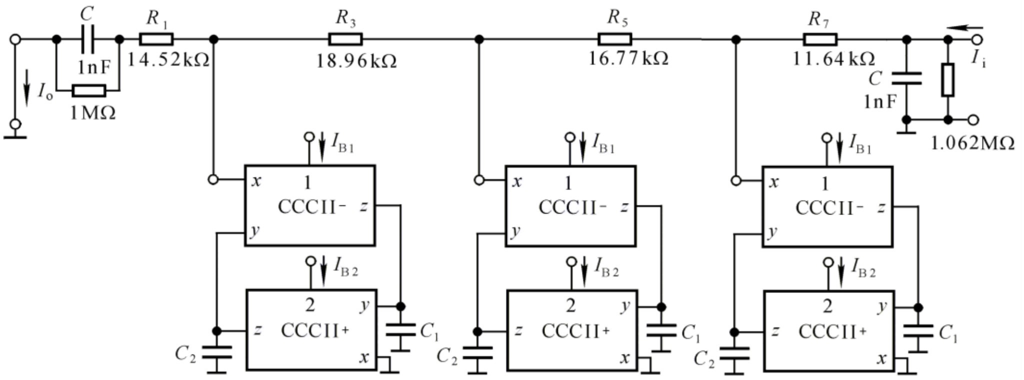

Fig. 6 – Seventh-order 0.28/60dB low-pass Cauer filter employing CCCIIs. Leftmost: $I_{B1}$ = 8.448 μA, $I_{B2}$ = 25.35 μA; center: $I_{B1}$ = 1.690 μA, $I_{B2}$ = 35.76 μA; rightmost: $I_{B1}$ = 2.422 μA, $I_{B2}$ = 33.47 μA.

To adapt to actual frequencies to achieve the cutoff frequency $\omega_c$ to be designed, selecting $C$ = 1 nF, for the leftmost FDNR with a lossy resistance, from the second formula of (4), an appropriate impedance-scaling factor is given by $k_z = C_N/(C\omega_c) = 10.62\times10^3$. Then $R_1 = k_z\times1.367 = 14.52$ kΩ, $R_3 = k_z\times1.785 = 18.96$ kΩ, $R_5 = k_z\times1.579 = 16.77$ kΩ, $R_7 = k_z\times1.096 = 11.64$ kΩ. The scaling normalized lossy resistance value is $R_{X1} = k_zV_T/2I_{B1}$. The scaling normalized bias currents from (3) and (4) can be written as

$$I_{B1}=I_{NB1}/k_z,\ I_{B2}=k_z\omega_c^2\frac{C_1C_2}{C_{N1}C_{N2}}I_{NB2}. \tag{5}$$

Here $I_{B1} = 89.72\times10^{-3}/k_z = 8.448$ μA. Picking $C_1 = C_2 = 5$ nF to make the value of $I_{B2}$ appropriate, then $I_{B2} = 10.62\times10^3\times6.28^2\times15^2\times10^6\times1\times10^{-18}\times10.77\times10^{-3} = 25.35$ μA.

Similarly, the remaining FDNR, including a lossy resistance, can also be calculated, as given in Fig. 6. To avert loading problems at input and output terminals, two current buffers at the input and the output can be used. However, for circuit brevity, the two buffers have been left out. To set a dc path for the circuit, a 1 MΩ resistance is used at the output terminal, which shunts with $C$ at the output. To ensure the realization of a gain of 0.5, this resistor must be counterbalanced by a 1.062 MΩ resistance shunting with $C$ at the input. The adoption of two large resistors does not affect the performance of the filter in interesting frequency ranges.

## 4. CHECK WITH MULTISIM

To verify the performance designed circuit, the sub-circuit for bipolar CCCII, according to Fig. 4 in [32], is established by using transistor PR100N and NR100N in the Multisim software, and then the circuit of Fig. 6 is established. At last, the circuit of Fig. 6 using ±1.5 V power supply is simulated. The results from alternating current (ac) simulation and Monte Carlo (MC) simulation, using 5% tolerance of capacitances, resistances, and BJT area, are indicated in Fig. 7, which gives subtle differences. Using the cursor of the Multisim finds the actual values: $A_{min}$ = 60.34 dB > 60 dB when $f_s$ = 17.78 kHz; $A_{max}$ = 6.16 dB > 0.28 dB when $f_c$ = 15 kHz.

A magnified view of the pass-band frequency plots for Fig. 7 is demonstrated in Figs. 8 and 9 shows a magnified view of the transition band and stop band amplitude-frequency characteristics of Fig. 7.

The transient analysis for the designed seven-order low-pass Cauer filter is indicated in Fig. 10. When a sinusoidal signal with an amplitude of 20 μA and a frequency of 10 kHz is added at the input of the filter, the output amplitude under a steady state shows approximately 9 μA, phase shift $0^0$. Fig. 11 shows the transient analysis when $I_i$ = 20 μA, $f$ = 20 kHz. The output amplitude under a steady state is about 0.12 μA, and the phase shift is about $90^0$.

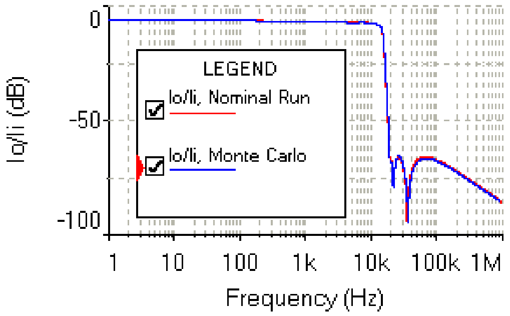

Fig. 7 – Amplitude-frequency characteristics of Fig. 6.

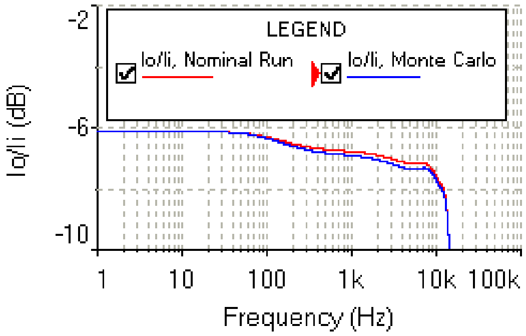

Fig. 8 –Magnified pass-band details of Fig. 7.

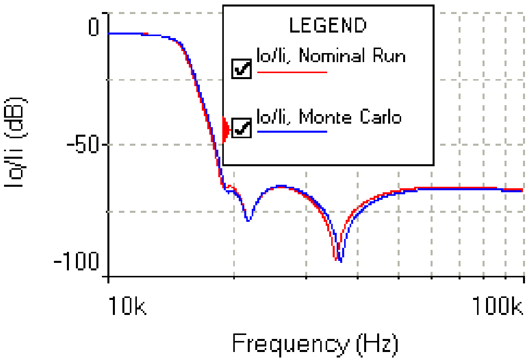

Fig. 9 – Transition-band and stop-band details of Fig. 7.

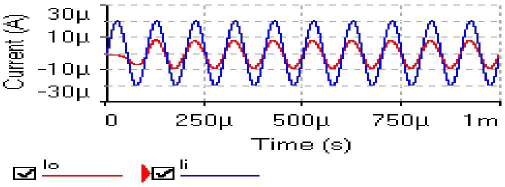

Fig. 10 –Transient analysis for the filter using $I_i$ = 20 µA, $f$ = 10 kHz.

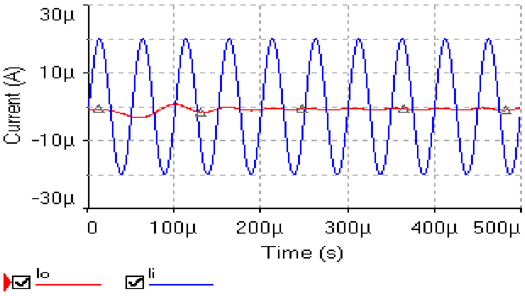

Fig. 11 –Transient analysis for the filter using $I_i$ = 20 µA, $f$ = 20 kHz.

In a word, the simulation results for the circuit are consistent with the theory.

## 5. **CONCLUSIONS**

Without a doubt, the performance of the simulated FDNR can be no better than the resistances, capacitances, and CCCIIs employed in their simulation. Deviations appearing in the simulation are inevitable. However, the designed circuit employs only grounded capacitors and six CCCIIs and does not require any matched conditions. Its performance, if desired, can be slightly regulated by adjusting bias currents in the CCCIIs. This filter can be used in communications, instrumentation, and measurement systems, for example, sharp-cutoff smoothing filters in the audio D/A converters. The main disadvantage of the circuit is the adoption of two large resistors, which is not conducive to the realization of integrated circuits.

We look forward to hearing improvement suggestions from relevant scholars to research this filter.

## ACKNOWLEDGEMENTS

This work is supported by the Natural Science Foundation of Shaanxi Province, China (Grant No. 2017JM6087). The author would also like to thank the anonymous reviewers for their suggestions.

*Received on 8 June 2021*

## REFERENCES

1. C. Chang, M.N. Swamy, *Analytical synthesis of odd/even nth-order elliptic Cauer filter structures using OTRAs*, Int. J. Circuit Theory Appl., **41**, *12*, 1248–1271 (2013).
2. Z. Hou, S. Shen, Y. Ye *et al.*, *Research on the linear acceleration sensor signal acquisition technology based on the high-order anti-aliasing Cauer filter*, J. Circuits, Syst. Comput., **29**, *1*, 2050008 (2020).
3. J.A.G. Malherbe, *Wideband bandpass filter with extremely wide upper stopband*, IEEE Trans. Microwave Theory and Techniques, **66**, *6*, 2822–2827 (2018).
4. M. Hayati, F. Shama, *A compact lowpass filter with ultra-wide stopband using stepped impedance resonator*, Radioengineering, **26**, *1*, 269–274 (2017).
5. S. Woo, J.K. Cho, *A switched-capacitor filter with reduced sensitivity to reference noise for audio-band sigma-delta D/A converters*, IEEE Trans. Circ. Syst. II: Express Briefs, **63**, *4*, 361–365 (2016).
6. Y. Xu, P.R. Kinget. *A switched-capacitor RF front end with embedded programmable high-order filtering*, IEEE J. Solid-State Circuits, **51**, *5*, 1154–1167 (2016).
7. C.M. Chang, S.H. Tu, M.N.S. Swamy, et al, *Design of odd nth-order elliptic high-pass filters employing OTRAs*, IET Circuits Dev. Syst. **13**, *2*, 174–184 (2018)
8. A.B. Bogatyrev, S.A. Goreinov, S.Y. Lyamaev, *Analytical approach to multiband filter synthesis and comparison to other approaches*, Problems of Information Transmission, **53**, *3*, 260–273 (2017).
9. S. Jha, *Voice signal separation from train noise corrupted signal using notch and elliptic filter*, Int. J. Electr. Eng. Tech., **11**, *3*, 218–230 (2020).
10. S. Franco, *Design with operational amplifiers and analog integrated circuits*, fourth edition, Mc. Graw-Hill Science Engineering, 2014.
11. S.S. Borah, M. Ghosh, A. Ranjan, *Higher order multifunction filter using current differencing buffered amplifier (CDBA)*, Rev. Roum. Sci. Techn. – Électrotechn. et Énerg., **67**, *1*, 59–64 (2022).
12. Y.A. Li, *A modified CDTA (MCDTA) and its applications: designing current-mode sixth-order elliptic band-pass filter*, Circuits Syst. Signal Process., **39**, *5*, 670–672 (2009).
13. Y.A. Li, *Current-mode sixth-order elliptic band-pass filter using MCDTAs*, Radioengineering, **20**, *3*, 645–649 (2011).
14. M.S. Diab, A.M. Soliman, *Balanced ota-c elliptic Cauer filters for biomedical applications*, 41st International Conference on Telecommunications and Signal Processing (TSP), IEEE, 2018.
15. M.S, Diab, S. Mahmoud, (2018, November). *Elliptic OTA-C Low-pass filters for analog front-end of biosignal detection system*, International SoC Design Conference (ISOCC), IEEE, 2018, pp. 103–104.
16. A. Fabre, O. Saaid, F. Wiest et al, *High frequency applications based on a new current controlled conveyor*, IEEE Trans. Circuits Syst. I, Fund. Theor. Appl., **43**, *2*, 82–91 (1996).

17. Y.A. Li, Y.H. Xi, Z.T. Fan *et al*,, *Systematic synthesis of second generation current-controlled conveyor-based Tow-Thomas filters with orthogonal tune of pole frequency and quality factor*, Rev. Roum. Sci. Techn. – Électrotechn. et Énerg., **62**, *1*, 76–81 (2017).
18. D. Agrawal, S. Maheshwari, *High-performance electronically tunable analog filter using a single EX-CCCII*, Circuits Syst. Signal Process., **40**, *9*, 1127–1151 (2021).
19. A. Yesil, Y. Babacan, *Design of memristor with hard-switching behavior employing only one CCCII and one capacitor*, J. Circuits, Syst. Comput, 2021.
20. D. Agrawal, S. Maheshwari, *Electronically tunable grounded immittance simulators using an EX-CCCII*, Int. J. Electron. **107**, *10*, 1625–1648 (2020).
21. Y.A. Li, B. Chen, *Systematic synthesis for second generation current control conveyor-based admittance converters,* Rev. Roum. Sci. Techn.–Électrotechn. et Énerg., **64**, *4*, 377–382 (2019).
22. D. Agrawal, S. Maheshwari, *Current mode filters with reduced complexity using a single EX-CCCII*, AEÜ-Int. J. Electron. Commun., **80**, *10*, 86–93 (2017).
23. F. Sen, A. Kircay, *MO-CCCII based current-mode fractional-order universal filter*, J. Circuits, Syst. Comput., **30**, *8*, art. 2150132 (2021).
24. D. Agrawal, S. Maheshwari, *Cascadable current mode instrumentation amplifier*, AEÜ-Int. J. Electron. Commun., **94**, *9*, 91–101 (2018).
25. S. Maheshwari, *Voltage-mode full-wave precision rectifier and an extended application as ASK/BPSK circuit using a single EXCCII*, AEÜ-Int. J. Electron. Commun., **84**, *2*, 234–241 (2018).
26. T. Kunto, P. Prommee, *Realization of tunable elliptic low-pass filter based on CCCIIs*, 2015 International Symposium on Intelligent Signal Processing and Communication Systems (ISPACS), 2015, pp. 331–336.
27. J. Koton, J. Jerabek, N. Herencsar *et al*., *Current conveyors in current-mode circuits approximating fractional-order low-pass filter*, 2017 European Conference on Circuit Theory and Design (ECCTD), 2017, pp. 1–4.
28. N. Chomnak, S. Srisamranrungrueang, N. Wongprommoon, *Simulating Elliptic Low-pass Filter based on MOCCCII,* IOP Conference Series Materials Science and Engineering, 2020, pp. 012037.
29. Y.A. Li, *Realization of seventh-order Chebyshev active low-pass filter,* Recent Advances in Electrical & Electronic Engineering, **15**, *1*, 67–74 (2022).
30. Y.A. Li, *Systematic Synthesis for electronic-control LC oscillators using CCCIIs*, Rev. Roum. Sci. Techn. – Électrotechn. et Énerg., **63**, *1*, 71–76 (2018).
31. M.T. Abuelma'Atti, N.A. Tasadduq, *Electronically tunable capacitance multiplier and frequency-dependent negative-resistance simulator using the current-controlled current conveyor*, Microelectron. J., **30**, *9*, 869–873 (1999).
32. M.T. Abuelma'Atti, M.A. Al-Qahtani, *A new current-controlled multiphase sinusoidal oscillator using translinear current conveyors,* IEEE Trans. CAS-II, **45**, *7*, 881–885 (1998).